Design and Methods of Construction of a Biomimetic Inspired Carbon Fiber Wing

Gonçalo Martins de Almeida
goncalomdalmeida@gmail.com

Instituto Superior Técnico, Universidade de Lisboa, Portugal

December 2019

Abstract

This project focuses on the concept of biomimicry and the implementation of animal design in aircrafts. It begins by listing and explaining several designs found in nature that could be used to improve modern engineering, specifically in the aerospace industry. Later, the concept of leading-edge serrations is chosen to be further studied. Using CATIA V5, the design of a carbon fiber wing is developed containing an actuator that creates the leading edge serrations. The original wing is modified and several components and mechanisms necessary to make it work were added. The wing and all its main components are developed in carbon fiber prepreg. Both new and original wings are subjected to structural analysis with different pressures and loads and the results were compared to assess if the modifications were viable or would pose a structural risk. For last, the methods and procedures to construct the wing and all its components in carbon fiber is presented. This is done using resin moulds and CNC Jigs and all the necessary hardware required to center and fix the parts in place.

Keywords: CATIA V5, Carbon fiber prepreg, Structural Analysis, Moulds, CNC Jig

1. Introduction

There is an ever-going pursuit of efficiency and innovation in the aerospace industry, whether that might be due to high costs of fuel or simply to reduce operating cost and CO_2 emissions. Nature has, for millions of years, perfected biological designs that allow species to proliferate and thrive over the conditions they were given. For this reason, engineers have been looking into nature for inspiration when developing new technology.

2. Biomimicry

Biomimicry is an approach to innovation that seeks inspiration in nature by emulation its time-tested design.

2.1. Drag Reduction

2.1.1. Fish slime. Lotus leaf. Self-cleaning

The slime fish secrete through their pores is a combination of polysaccharides, lipids and lipoproteins that enter the boundary layer and fill irregularities of the surface, improving streamlining. Most importantly, the slime has a lower viscosity than the water around the fish, this helps to reduce the frictional shear stresses arising from the “stickiness” or viscosity of water [1].

Lotus leaves surface have a hierarchically rough structure that discourages wetting, making it very hydrophobic [2]. This surface has uneven heights of papillae that decrease water adhesion due to unfavorable surface interactions between water and leaf. These hydrophobic characteristics allow the lotus to clean itself when water falls on its leaves. The debris are pickup by the rolling droplets and carried away from the plants surface.

Gliders, due to their non propulsion characteristics, depend heavily on maintaining a high level of lift with the lowest drag possible. This can be a problem since they usually fly at low altitudes where bugs and dirt deposits on the aircraft surfaces are common. For this reason, they are more susceptible to wing contamination than any other type of aircraft.

Every piece of dirt/bug in the leading-edge creates disturbances in the laminar flow causing early transition to turbulent flow and inducing separation. A wing surface coated with a hydrophobic material would allow water droplets to agglomerate and roll off the wing carrying away the surface debris.

2.1.2. Skin ripples. Dolphins

Dolphins can delay the transition to turbulent flow using their soft, compliant skin and thus reducing skin friction drag. The viscoelastic properties of the skin interact with the flow over the body as a viscous damper and absorb energy from pressure oscillations called "Tollmien-Schlichting waves" that force the boundary layer to go turbulent. Dolphins sense these pressure oscillations using canal neuromasts and activate control micro vibrations to produce skin vibrations of up to 5mm amplitude at around 10Hz that destructively interfere with the Tollmien-Schlichting pressure waves. With this method, dolphins can delay the transition to a turbulent boundary layer and prevent boundary layer separation in the back allowing the front to maintain a laminar flow [3].

2.1.3. Shark skin. Dermal denticles

Shark skin is composed of dermal denticles in an overlapping diamond shape that form grooves and channels. Denticles reduce drag and turbulence with their flow channeling capability because turbulent boundary layer on a surface with longitudinal ribs originates less shear stress, and consequently less drag than the same profile with a smooth surface. Denticles aligned with the flow prevent lateral transfer of momentum and result in a more gradual velocity profile with less shear stress.

Boundary layer separation is initiated by a flow reversal in the boundary layer, meaning that the flow locally flows opposite to the direction of motion. At this moment, the flow reversal forces the scales to lift, acting as vortex generators, this energizes the boundary layer pushing the fluid towards the skin. This way the shark can reattach the flow and reverse the separation [4].

2.1.4. Whale protuberances. Tubercles

An adult humpback whale can be as long as 15m and 30 metric ton yet capable of doing a 360° turn in under 10m radius when hunting. This maneuverability has been attributed to leading edge protuberances on its flippers. In a wind tunnel study conducted by Miklosovic et al. [5] two fin designs were approached, a typical whale fin with protuberances and one baseline without. The results reported an increase of 6% in maximum lift over the baseline and a 40% increase in stall angle by the fin with protuberances. A decrease in drag was also seen over the AoA range of $10° \leq \alpha \leq 18°$ in the fin with protuberances as well as an increase of lift to drag ratio for $\alpha \leq 10°$ and $\alpha \geq 12°$. In this test, a fin with protuberances is able to delay the stall angle from 12° in the baseline to around 17°. Drag also decreases from $10° \leq \alpha \leq 18°$, this means that the concept of protuberances is advantageous for high angles of attack.

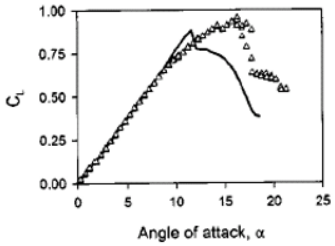

Figure 1: Miklosovic tests [15]; Δ(fin w/protuberances); -(No protuberances).

The serrated effect of a leading edge with protuberances creates a series of valleys and peaks. Because of this, a series of vortexes are created at each peak and travel towards the valley. These vortexes create low pressure zones along the foil and are responsible for generating the added lift in a post-stall regime. In Derrick Custodio [6], a comprehensive study of the effect of leading-edge protuberances in dynamic forces was carried out using several combinations of serrations. These tests were made using 4 and 8 protuberances and several amplitudes for each one of them, from small amplitudes (S), medium (M) to large (L).

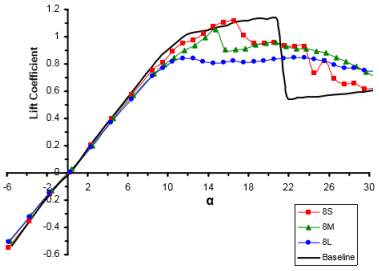

Figure 2: Results obtained by Custodio [18] for 8 protuberances and λ=0.25c.

Results showed early separation caused by the induced vortexes created by the protuberances, however this separation is momentary as it quickly reattaches and stabilizes at $\alpha \approx 15°$. This means that protuberances are detrimental during standard flight at low angles of attack (pre-stall) but would be advantageous during high angles of attack (heavy banking or rapid ascends), when the baseline airfoil is stalling. The design of the protuberances also contributes for different results, a larger amplitude results in less pre-stall lift and more post-stall lift.

To take full advantage of the protuberances, a wing would remain with a baseline airfoil for most of the flight and would activate protuberances once a rapid maneuver (over $\alpha \geq 22°$) was necessary.

2.1.5. Tip morphing. Winglets

Winglets were first developed by Richard T. Whitcomb in the 1970's by looking at how birds flexed their wing tips

during flight. The high pressure beneath the wing forces the air to flow upwards, towards the low pressure. This causes vortexes that increase the induced drag. Forcing air to flow around the winglet increases the radius of those vortexes which translate into less energetic vortexes easier to dissipate [7]. This reduces the turbulence in the wake of the wing which allows for lower induced drag and for the runway to be cleared of turbulent flow more rapidly. Winglets are advantageous at low speeds where induced drag is high. However, they increase parasitic drag and become less necessary at high speeds where this component is more prevalent. For this reason, a morphing tip would be the ideal solution. Winglets would be activated during take-off and would retract when parasitic drag overcomes the induced drag.

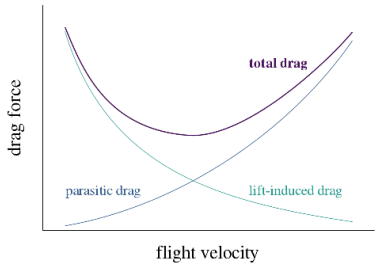

Figure 3: Drag components.

2.2. Types of Wings

2.2.1. Elliptical wings

Elliptical wings can be found in most small birds with high maneuverability. These have high degree of control and maneuverability in confined spaces; minimized drag for rapid ascend and descend; slotted between the primary feather, prevents stall during sharp turns [8]; and adapted to low speed flights. These characteristics make it an ideal wing template for high maneuverable planes or short distances commuters such as the Supermarine Spitfire and the VH2 Streamline.

2.2.2. High speed wings

High speed wings are usually found in prey birds, as these animals require sudden burst of speed to catch prey. They are not suited for low speed flights; tapered for high speed with low drag and energy consumption; and adapted for long migration birds with long wing bones. These trades make them common in aircraft fighters and fast commuters who require fast flights and rapid changes in direction.

2.2.3. Long soaring wings

Long gliding wings are easily identified by their long wingspan and short relative chord. Their high aspect ratio increases the lift-to-drag ratio, vastly improving energy efficiency. They are characterized by being adapted for high speeds and dynamic soaring; less maneuverability; and ideal to glide over large expanses of water using sea winds and thermals. These characteristics make the long soaring wings and ideal feature for gliders and highly efficient commercial aircrafts.

2.2.4. High lift and broad soaring wings

This type of wing is present in some of the heaviest and larger prey birds on the planet. They are broad and relatively long wings; capable of take-off and landing in confined areas; capable of high lift, low speed soaring and slow descents; good maneuverability for tactic soaring in air currents over land; present in prey birds such as vultures, hawks, ospreys, pelicans, eagles, etc. These are all great characteristics when design a large plane capable of carrying heavy weights for long distances such as cargo planes and large commercial aircrafts.

3. Leading edge serrations applied to a wing

This chapter approaches the application of leading edge serrations to a selected aircraft, the dynamic characteristics of this aircraft wing are studied in order to create a baseline for further modifications. It is also proposed several concepts of actuators to create the leading edge serration.

3.1. Standard wing specification

The aircraft chosen to be the focus of this application was the Tekever AR5 Evolution, it has a simple airfoil (Selig S4233) that is very similar to a cross section of a humpback whale fin.

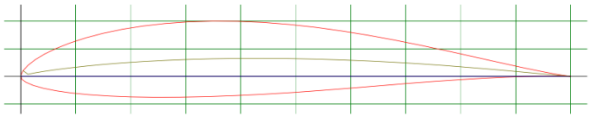

Figure 4: Airfoil S4233.

Tekever	**AR5 Evolution**
Wingspan	4.3 m
Length	3 m
Chord	0.4 m
Cruising speed	140 km/h
Max speed	150 km/h
Weight (empty)	100 kg
MTOW	150 kg
Endurance	8 to 12 hours
Range	1400 km

Table 1: AR5 Evolution specs, [9].

For a fixed chord of $c = 0.4m$, a cruising speed of $U = 140\ km/h = 38.89\ m/s$ and an air kinematic viscosity

of $v_{air} = 1.51 \times 10^{-5} m^2/s$ the Reynolds number can be calculated for a typical operation.

$$Re = \frac{U \cdot c}{v_{air}} = \frac{38.89 \times 0.4}{1.51 \times 10^{-5}} = 10^6 \qquad \text{(Eq. 1)}$$

Once the Reynolds number is known the C_l can be calculated and plotted.

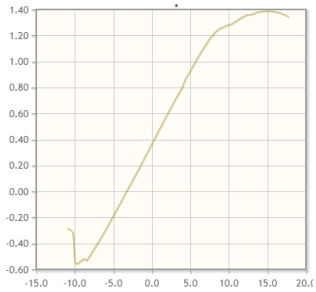

Figure 4: Cl v α, $Re = 10^6$

From these results, a maximum of lift coefficient $C_l = 1{,}4$ is obtained at an angle of attack of α=15°. This wing has a high aspect ratio, for this reason the tridimensional effects of tip vortexes are not so significant. Since the wing has no torsion and α is constant along the wingspan then α_{ef} is also constant along the wingspan and $C_{L2D} \approx C_{L3D} = C_L = 1{,}4$ can be assumed. The maximum lift extractable from this wing can be calculated from,

$$L_{max} = \frac{1}{2} \rho U^2 S C_l \qquad \text{(Eq. 2)}$$

Where L_{max} is maximum lift, the air density $\rho = 1{,}225 kg/m^2$, $U = 150\ km/h = 41{,}67\ m/s$ is speed, and wing area $S = wingspan \cdot chord = 4{,}3 \cdot 0{,}4 = 1{,}72 m^2$.Maximum lift obtainable is then $L_{max} = 4898{,}7N$. An aircraft structure is designed to be able to withstand the forces acting upon its wings and fuselage. For this extreme situation of maximum lift, the load factor is calculated.

$$n_{max} = \frac{L_{max}}{W} \qquad \text{(Eq. 3)}$$

Where the weight is $W = MTOW \cdot g = 150 \cdot 9{,}8 = 1470N$. The maximum load factor is then $n_{max} = \frac{4898{,}7}{1470} = 3{,}33$. This situation is inside the 'Structural Damage' realm and is not advised to be operated in. Less extreme loads are expected for the wing to be operated in. However, because these are the loads experienced in high angles of attack near the stall regime, they do need to be taken in consideration when developing the modified wing.

A more typical operation would be an aircraft traveling at $U = 25 m/s$ activating its flaps and reaching a near stall angle of attack of α=15°, resulting in a $C_l = 1{,}4$ a lift of $L = 1763N$ and a load factor of $n_{to} = \frac{1763}{1470} = 1{,}2$. At this point, it would be required to activate the protuberances, allowing for an extension of lift in a stall regime. In this situation, each wing is experiencing a load of $L/2 =$ 881,6N, which for a wing area of $S/2 = 1{,}72/2 = 0{,}86 m^2$ equates to roughly 500N applied per square meter.

This will be the benchmark for the structural analysis the modified airfoil will be subjected to. Because there is no information on which type of structural members the Tekever wing has inside, the analysis will only be conducted with the exterior airfoil without ribs nor spars. To ensure that even the exterior surface is well designed and capable of withstanding flight loads a factor between 10% to 20% of the loads expected in operation will be applied. The tests will then be conducted with a range of pressures applied (from $P_1 = 100N/m^2$ to $P_5 = 200N/m^2$) to analyze where and how the structure will buckle and deform, and a distributed force analysis of $F_1 = 100N$ and $F_2 = 200N$ to simulate a flight load situation.

3.2. Proposed actuation

The protuberances in a leading edge of a wing are not beneficial for most of the time, during standard flight mode this feature would increase drag and decrease lift for small angles of attack. For this reason, protuberances in the leading edge of a wing should only be activated when needed, during sharp turns or steep climbs.

3.2.1. Types of actuator design

Type1, consists of a deformable leading edge made of an elastic membrane. This membrane gets deformed by a carbon fiber rod with several protuberances along its longitudinal length, similar in shape and form as a camshaft in an engine. In its OFF position these protuberances are inside and not in contact with the elastic membrane, during this state the wing has its normal shape. In its ON position the actuator rotates 180° along its axis and the protuberances push the elastic membrane outwards creating a serrated effect on the leading edge.

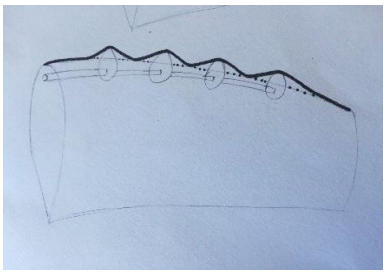
Figure 5: Type1, actuator engaged.

Type2, has the same principle as the first but without the elastic component. The protuberances are created by solid movable parts integrated in the wing geometry. The rotation of triangular shaped parts would create the serrated effect in the leading edge of the wing.

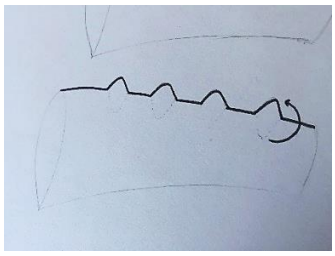

Figure 6: Type2, actuator engaged.

Type3, consists of a similar approach as type1 but instead of a camshaft actuator that rotates inside an elastic membrane there are several hydraulic actuators along the leading edge of the wing. These hydraulic pistons would push the elastic membrane outwards creating the protuberances intended.

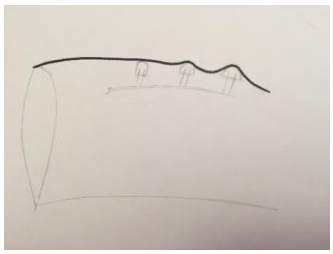

Figure 7: Type3 actuator design.

3.2.2. Chosen actuator design

After evaluating all three types the first one stood out as the best balance between versatility, innovation and feasibility. If designed properly, this configuration would not compromise the wings structural rigidity and would not increase its total weight. The elastic membrane would however pose a complex engineering problem since it would have to endure harsh environments, while maintaining its elasticity and integrity.

Most of the improvements associated with leading edge serrations are due to its effect close to the tip of the wing, for this reason, the actuator is mounted from the midpoint of the wingspan up to the tip.

4. CAD Development

4.1. Parts construction

The modified wing is comprised of six carbon fiber components, one thermoplastic support, one aluminum insert and one elastic membrane covering the deformable leading edge. All these components combine, allow the developed wing to create eight protuberances in the leading edge when an electric motor is activated. Bellow, a complete assembly and an exploded view of the components can be seen.

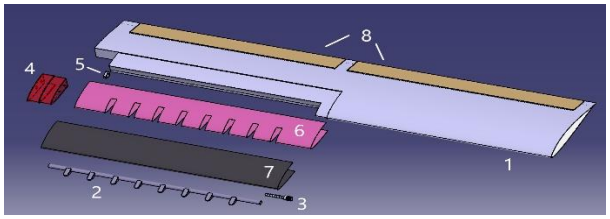

	Name	Material
1	Airfoil	Carbon Fiber 2,4mm thickness
2	Camshaft Actuator	Carbon Fiber 2,4mm thickness
3	Camshaft Gear Insert	Aluminum
4	Actuator Lock	Carbon Fiber 2,4mm thickness
5	Plastic Insert	Thermoplastic
6	Armature	Carbon Fiber 1,5mm thickness
7	Elastic Membrane	Elastic component 1,5mm
8	Flaps	Carbon Fiber 2,4mm thickness

Table 2: List of components.

4.1.1. Airfoil

The material chosen was prepreg carbon fiber with a 2.4mm (0.093'') thickness and a ±45° twill.

Carbon Fiber	**Prepreg**
Thickness	2.4 mm
Young Modulus	$7 \cdot 10^{10}\ N/m^2$
Poisson Ratio	0,1
Density	$1600\ kg/m^3$
Yield Strength	$1.85 \cdot 10^{9}\ N/m^2$
Thermal Expansion	$2.1\ K^{-1}$
Twill	+/-45°

Table 3: Carbon Fiber Prepreg specifications [28].

The thickness chosen is a structural one, and the material properties make it capable to withstand strong loads. However, because there is no information available of what type of structural components the Tekever wing has, it was not included any spars or ribs into this design. Once the airfoil was plotted the original wing from Tekever could be constructed, it can be seen bellow without the winglets and the flaps assembled.

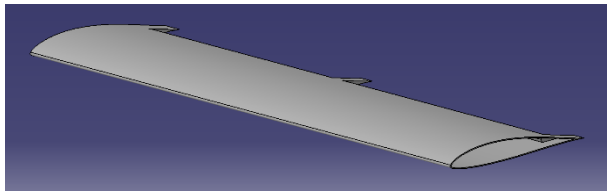

Figure 8: Original wing in CATIA V5.

A Von Mises stress analysis was developed for several pressures applied on the wing surface, $100 N/m^2$,

$150N/m^2$, $160N/m^2$, $170N/m^2$ and $200N/m^2$ respectively. By applying a uniform pressure on the airfoil, it is possible to see where the weak points of the structure are, and where it can be improved. As well as where it is more prone to deform.

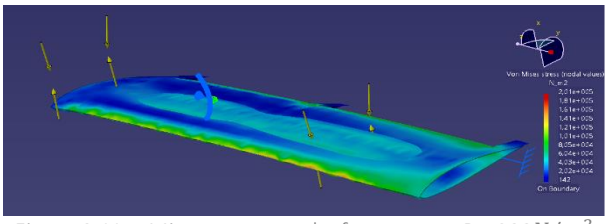

Figure 9: Von Mises stress results for pressure P_5=$200N/m^2$ applied to original wing.

At a pressure of $150N/m^2$ some deformation becomes apparent and from $160N/m^2$ onwards a 'bubble' is visible where delamination of the carbon fibers would probably occur if this wing was used with no internal structural elements. The thickness of 2,4mm would not be enough to endure these types of stresses, further development on internal structural reinforcement would be required, weather spars and ribs or simply a structural foam. Stress concentration can be seen at the leading edge near the root of the wing and where the flaps are mounted, but it is overall well distributed along the wing.

From the original wing several modifications were made at the leading edge and tip to accommodate the actuator mechanism. The 2,4mm thickness remains the same.

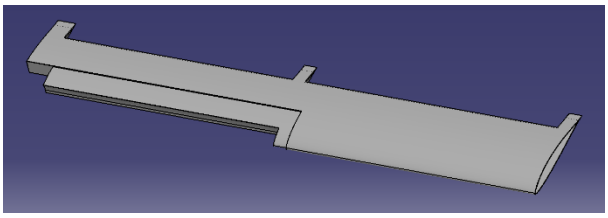

Figure 10: Modified wing.

The same Von Mises stress analysis was carried out for this wing to compare any loss or gain in structural integrity.

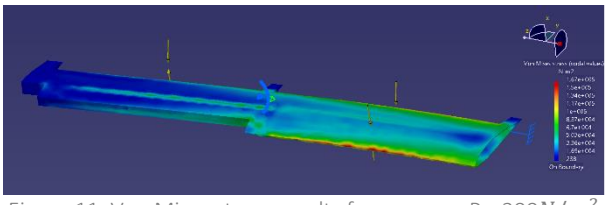

Figure 11: Von Mises stress results for pressure P_5=$200N/m^2$ applied to modified wing.

The modified area now handles the stress much better due to its 'step' like shape, adding to its structural rigidity. Also, there is minimal increase of displacement compared with the original wing. This is a good thing as some components will have axial movement that require minimum warp to function properly. No potential delamination is visible, even at the highest pressure applied of P_5=$200N/m^2$.

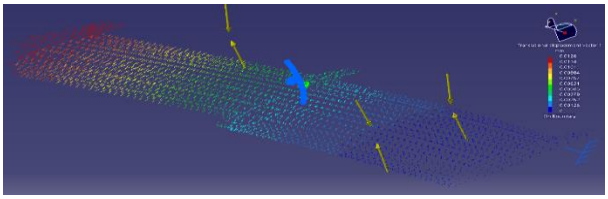

Figure 12: Translational Displacement Analysis of modified wing, P_5=$200N/m^2$.

Maximum displacement occurs at the same places as before (wing tip) with slightly higher values. But still no bigger than x=0.0126mm of displacement at the most distorted region for P_5=$200N/m^2$. In the preliminary wing the displacement had a backward direction, towards the trailing edge, while in the new design, the distortion has a forward direction, towards the leading edge.

The modified wing was then assembled in CATIA with an internal structural foam (also used as mould) in order to conduct the same tests. The foam selected was FV699 sourced from General Electric Plastics [10] due to its flame resistant and lightweight properties when compared with other foams. The same pressure analysis was conducted with P_1=$100N/m^2$ and P_5=$200N/m^2$ for a comparison on how the wing would benefit with an interior structure. The highest concentration of stress is now located closer to the root of the wing, with maximum values found at the trailing edge. Stress values were significantly reduced when compared with the previous iterations of wings.

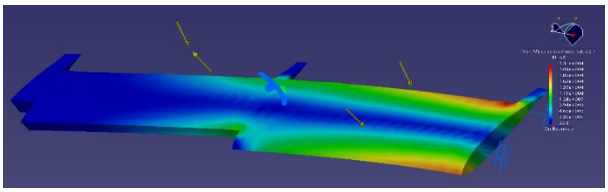

Figure 13: Von Mises stress results for pressure P_5=$200N/m^2$ applied to modified wing with structural foam

When comparing stress values for P_1=$100N/m^2$ with previous iterations it is noted a reduction in maximum stress of 87,3% between the modified wing with structural foam and the original wing with no internal structure. And a reduction of 86,2% between the modified wing with structural foam and the modified wing with no internal structure. Similar reduction values are obtained for P_5=$200N/m^2$.

The displacement values obtained were far smaller than the previous wing iterations. A maximum displacement,

at the leading edge, of x=0,00133mm for P_1=100N/m^2 and x=0,00266mm for P_5=200N/m^2 represent a reduction in displacement of 78,9% between modified wing with structural foam and no foam. And a 71,6% displacement reduction between modified wing with structural foam and the original wing. A preliminary upper surface load was chosen, this load will enhance the worst-case scenario, despite not accurately portraying a real situation. Two resultant loads were applied, F_1=100N and F_2=200N. The distributed force mimics a uniform force applied to a half wing with a uniform distribution, in a real situation a wing would experience a nonuniform distribution of force. However, this uniform distribution allows the analysis to be more of a 'worst-case scenario' as a larger amount of force is applied to the tip of the wing when compared to, for example, an elliptical distribution. This creates larger amounts of moment experienced by the root of the wing and a larger amount of deformation at the tip.

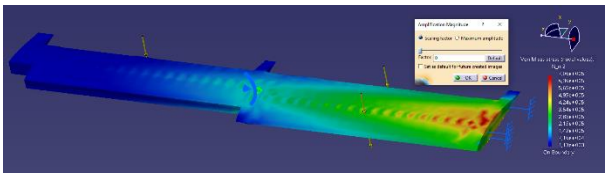

Figure 14: Von Mises stress results for distributed force F_2=200N applied to modified wing with structural foam.

Stress is concentrated at the root of the wing, with maximum values of $7{,}06 \cdot 10^5\ N/m^2$ and $1{,}41 \cdot 10^6\ N/m^2$ for F_1 and F_2, respectively. While the displacement results showed maximum distortion at the tip, with maximum values of 0,377mm and 0,755mm for F_1 and F_2, respectively.

	Original Wing	Modified Wing	Modified Wing w/ structural foam
Max. Stress *(F_1=100N)*	$4{,}09 \cdot 10^6\ N/m^2$(at root)	$4{,}22 \cdot 10^6\ N/m^2$(at root)	$7{,}06 \cdot 10^5\ N/m^2$(at root)
Max. Stress *(F_2=200N)*	$8{,}17 \cdot 10^6\ N/m^2$(at root)	$8{,}45 \cdot 10^6\ N/m^2$(at root)	$1{,}41 \cdot 10^6\ N/m^2$(at root)
Max. Displacement *(F_1=100N)*	1,62mm (at tip)	1,73mm (at tip)	0,377mm (at tip)
Max. Displacement *(F_2=200N)*	3,25mm (at tip)	3,46mm (at tip)	0,755mm (at tip)

Table 3: Original and Modified wings results comparison.

This table compares results with analysis not mentioned before, such as distributed forces F_1=100N and F_2=200N applied to the first two iterations of the wing (Original and Modified). As well as their respective displacements when such loads were applied. Note that the displacement is downwards (direction of load applied) with a slight forward component. This forward component is hardly noticeable and does not pose a problem, however, if it did, it could be attenuated by reinforcing the leading edge with a 1.5mm ply of carbon fiber prepreg. Because the previous forces (F_1 and F_2) withstood better than previously assumed, a second analysis was conducted to see how the modified wing with structural foam and no internal spars nor ribs would behave under a typical operation and an extreme situation. For this situation the forces are applied in the lower surface with an upward direction, mimicking the lift acting upon the wing.

A typical operation, seen in chapter 3, would have a load factor (n=1,2) with a lift of $L_{to} = 1763N$. Assuming the lift distribution is rectangular instead of elliptical and symmetrical to both wings a distributed force of $F_{to} = {}^{1763}/_{2} \approx 880N$ is applied. While on an extreme situation the maximum load factor (n=3,3) was taken into equation and a maximum lift of $L_{max} = 4898{,}7N$. Again, assuming the lift distribution is rectangular instead of elliptical and symmetrical to both wings a distributed force of $F_{max} = {}^{4898{,}7}/_{2} = 2450N$ is applied. The analysis has preliminary mesh of 25mm in size and is refined to 10m and 5mm. A smaller mesh size would require too much computation effort and time from the machine, becoming prone to crash.

$F_{to} = 880N$	**Mesh: 25mm**	**Mesh: 10mm**	**Mesh: 5mm**
Max. Stress *[N/m^2]*	$6{,}35 \cdot 10^6\ N/m^2$	$2{,}29 \cdot 10^7\ N/m^2$	$5{,}13 \cdot 10^7\ N/m^2$
Max. Displacement (tip) *[mm]*	3,32mm	5mm	5,51mm
Displacement at Camshaft Gear Insert *[mm]*	1,1mm	1,65mm	1,84mm

Table 4: Distributed Force Results, F=880N

$F_{max} = 2450N$	**Mesh: 25mm**	**Mesh: 10mm**	**Mesh: 5mm**
Max. Stress *[N/m^2]*	$1{,}77 \cdot 10^7\ N/m^2$	$6{,}25 \cdot 10^7\ N/m^2$	$1{,}43 \cdot 10^8\ N/m^2$
Max. Displacement (tip) *[mm]*	9,32mm	13,9mm	15,3mm
Displacement at Camshaft Gear Insert *[mm]*	3,32mm	4,59mm	5,1mm

Table 5: Distributed Force Results, F=2450N

The Yield Stress of the weakest material (Structural Foam) is $\sigma_{foam} = 5 \cdot 10^7\ N/m^2$ which is capable of withstanding the stress experienced in the internal part of the wing made of this material. With this in consideration, it is safe to say that if the wing was constructed using only the structural foam and no ribs and spars it would still be capable of withstanding the

loads applied in flight well inside the elastic deformation zone. However, there would be an advantage in assembling structural components to the structural foam when considering the distortion experienced at the tip. Or at least, redesign the structure for less displacement in this region. For the maximum load applied there is a displacement of 15,3mm at the tip and 5,1mm at the Camshaft Gear Insert, this is vertical displacement with minimal longitudinal displacement. If the Camshaft Actuator is too stiff and with no bending properties, there is a possibility to jam. For this reason, it's advisable that this component contains a longitudinal play when assembled as well as a play in the concentric rings it is supported on. This way, it will be able to move with the wings deformation and prevent jamming.

4.1.2. Camshaft Actuator

To make the leading-edge protuberances in the wing a *Camshaft Actuator* was developed in order to push the elastic membrane outwards, thus obtaining the desired serrated shape by rotation on its axis. In this application, each cam is 40mm long and 20mm wide, with a R10mm edge fillet on the side to accommodate the elastic membrane without tearing it. This design will locally increase wing chord on each cam by 14,824mm (0,037c). An amplitude of 7,412mm (0,01853c) in the serrated leading edge with a wavelength of 100mm and a frequency of 8cams per 720mm (11.1cams/m).

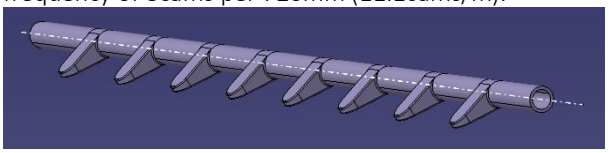

Figure 15: Camshaft Actuator.

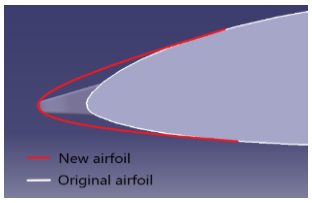

Figure 16: New and original airfoil comparison.

4.1.3. Camshaft Gear Insert

The *Camshaft Gear Insert* is the component that makes the connection between the carbon fiber actuator and the electric motor. This component is comprised of three parts, ***A*** - long corrugated area where the rod is laminated, the ridges provide good adhesive bond since the epoxy is placed in shear instead of peel; ***B*** – smooth and greased middle section that acts as a pivot; and ***C*** - geared section where the spur gear of the motor meshes, this was done with a 20° pressure angle and interlinked formulation so that the developer might change the gear ratios more easily in CAD .

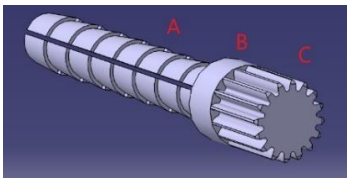

Figure 17: Camshaft Gear Insert sections.

4.1.4. Actuator Lock and Plastic Insert

The *Actuator Lock* is a carbon fiber component bolted to the *Airfoil* that locks the *Actuator Camshaft* in place. It contains a *Plastic Insert* made of thermoplastic glued to it, this secures the *Camshaft Actuator* in place restricting its longitudinal movement.

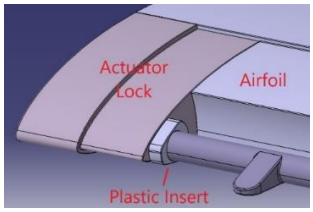

Figure 18: Local Assembly.

4.1.5. Armature and Elastic Membrane

The *Elastic Membrane* is a flexible component in the leading edge of the wing, this gets deformed when the *Actuator Camshaft* rotates creating the leading-edge protuberances.

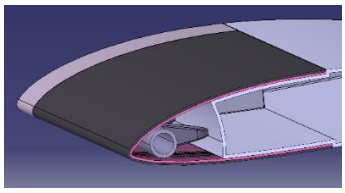

Figure 19: Elastic Membrane in black, section view.

The *Armature* is a thin carbon fiber (1,5mm thick) where the *Elastic Membrane* is glued in place, forcing it to maintain the airfoil shape during flight. It contains several slots on the leading edge to allow the cams of the *Actuator Camshaft* to pass through.

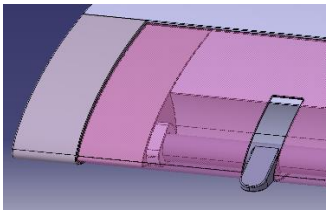

Figure 20: Armature Assembly.

4.2. Methods of Construction – Moulds and CNC Jigs

Prepreg Carbon Fiber consists of pre laminated sheets of carbon fiber embedded in epoxy resin that come in several thicknesses and lengths, depending on the customer needs. Developers can manufacture carbon fiber parts using resin, aluminum or even carbon fiber

moulds and patterns where the sheets of prepreg are laminated.

4.2.1. Airfoil Mould

To allow the airfoil to be made from a single piece, a three-piece mould process was developed (Figure 4.27). *Mould* ***A***, the *Interior Mould*, is made of a structural moulding foam where the carbon fiber is laminated over. After, both elements are placed on top of *Mould* ***C*** and enclosed with *Mould* ***B***, so that the carbon fiber acquires the outside shape it requires. Bolts and dowels between ***B*** and ***C*** respectively lock and center everything in position and the entire set up is sent to the autoclave to cure.

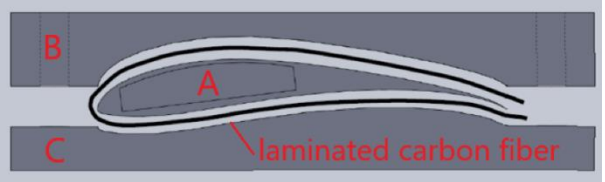

Figure 21: Three parts moulding scheme.

4.2.2. Camshaft Actuator Mould

The camshaft rod is laminated over the corrugated part of the *Gear Insert*, next the cam moulds must be glued to the rod. For this, the rod is placed on the *Camshaft Jig Base* and the cam moulds in the *Camshaft Jig Cover*, epoxy glue is applied at the circular surface of the cams and both jigs are bolted together.

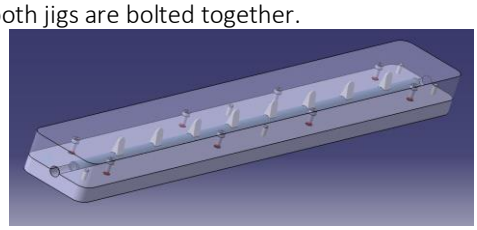

Figure 22: Camshaft Jig Assembly with centering dowels and bolts.

After this, the rod, now with the cam moulds glued in place, is removed from the jig and a 1,5mm thick ply of prepreg is laminated over the cam moulds.

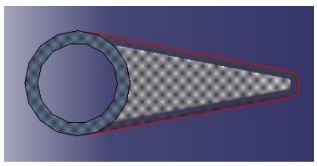

Figure 23: Lamination over cam moulds.

4.2.3. Actuator Lock Mould and CNC Jig

First step when developing a mould is to analyze the carbon fiber part and see if it's possible to laminate it in a one-piece mould. This is done by performing a '*Draft Analysis*', using the compass the developer can adjust the pulling direction and check if the part has any undercuts. In this case, a two-piece mould must be used as the carbon part is not able to exit a one-piece mould without destroying it. A *split surface* is necessary to divide the mould in half. Second step is to choose the *lamination surface*, in this case is the exterior surface. To lower cost production when developing moulds it's important to design them so that a 3 axis CNC machine can be used instead of a more expensive 4 axis. Also, resin blocks come in standard width dimensions (25mm, 50mm, etc.), for which the price increases with size.

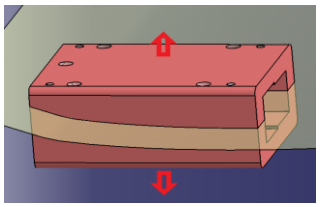

Figure 24: Mould divided by split surface

After lamination and curing the carbon fiber part is removed from the mould and placed in a CNC Jig whose main purpose is to hold the part in position to be cut and to assist the gluing process of the *Plastic Insert*.

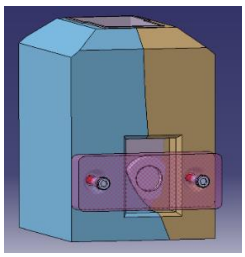

Figure 25: Actuator Lock CNC Jig

4.2.4. Armature Mould and CNC Jig

To construct the *Armature* a two-piece mould was created because a single piece mould would not allow the carbon fiber part to be extracted without damaging the assembly.

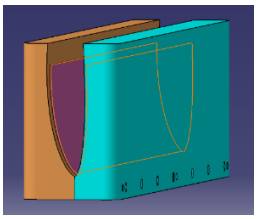

Figure 26: *Armature Mould*

After, the *Armature* is placed in a CNC Jig to cut the eight slots and glue the *Elastic Membrane* in place. Because the *Elastic Membrane* is meant to be glued on the exterior surface of the *Armature*, and to allow the milling drill to cut the slots, an interior jig must be used. In order to secure the *Armature* in place a vacuum jig was developed, this is achieved by incorporating a grid section fed by vacuum lines. Figure 28 shows in detail the orthogonal grid ***B*** where the *Armature* rests on. A ⌀4mm

O-ring is placed in a channel that seals the vacuum, marked with capture ***A.*** The vacuum lines are inserted in the side hole feeding both sides of the jig.

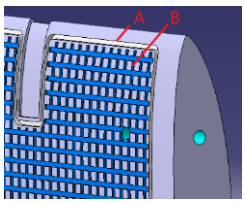

Figure 27: *Armature CNC Jig*

After milling, with the *Armature* still in place, a coat of glue is applied in its exterior surface and the *Elastic Membrane* is applied.

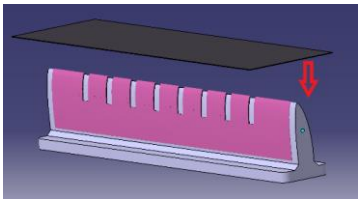

Figure 28: *Armature Mould*

5. Conclusion

5.1. Achievements

Stress analysis on concept type1 with internal foam structure showed that the new design would in fact reinforce the wing and make it capable of withstanding the loads applied in flight. It also showed that the components added to create the leading edge serration would not be compromised when loads were applied to the wing. A careful design took in consideration how the wing would deform and thus prevent the actuator mechanisms to lock and jam inside. From the distributed force tests and displacement analysis it was evident that the wing would tend to deform a considerable amount to risk jamming the interior mechanisms. For this reason, the camshaft actuator was developed in order to be secured in place by two concentric supports, the *Plastic Insert* with an aluminum ring and the *Gear Insert* section ***B***. This allows the shaft to be axially constrained, while maintaining a small degree of longitudinal freedom. The shaft is longitudinal constrained by the *Plastic Insert*, however, a small longitudinal play of 10mm at the gear insert mesh with the electric motor is advised for this component to slide along when the wing is deformed. This is to allow the *Camshaft Actuator* to move with the deformation of the wing.

5.2. Future Work

This project established and created a platform onto which future researchers can develop new iterations of leading edge serrations. The construction methods shed a light onto how moulds of carbon fiber parts are developed and was presented in a way that they can be modified and replicated in real life, giving the opportunity for future alumni to continue from where this project stopped. Further development on the electric motor that activates the *Camshaft Actuator* would be required. The selection of this component would have to take in consideration it is meant to be used at slow rpm's as the camshaft only requires 180° of rotation to be activated. The torque it applies would have to be taken in consideration as well, it should be great enough to rotate the camshaft and push the *Elastic Membrane* outwards without tear. For this reason, the *Camshaft Gear Insert* was developed with a CAD formulation of gears that can be easily manipulated for the best gear ratio with the electric motor.

Acknowledgments

I would like to give a special thank you to my family, specially my mother, for all the support through my academic life. To Miguel Passanha and the MPC Designworks team for all the knowledge I've acquired during my time working there, for what I am deeply grateful. Finally, to professor Filipe Szolnoky Cunha and professor João Oliveira for all the support and guidance for this thesis.

References

[1] Moe Wm. Rosen and Neri E. Cornford., Fluid friction of the slime of aquatic animals, Fleet Engineering Department, November 1970.

[2] Barthlott W, Neinhuis C., Planta. 1997;202:1–8. doi: 10.1007/s004250050096.

[3] Kramer M. O., The dolphins' secret, *New Sci.* 7 1118–20, 1960.

[4] Lang, A., et al., Bristled shark skin: a microgeometry for boundary layer control, Bioinspration & Biomimetics, 3, 1-9, 2008.

[5] Miklosovic, D. S., Murray, M. M., and Howle, L. E, Experimental Evaluation of Sinusoidal Leading Edges, Journal of Aircraft; Engineering Notes, Vol. 44, No. 4, pp. 1404-1407, July/August 2007.

[6] Custodio, Derrick, The effect of Humpback Whale-like Leading Edge Protuberances on Hydrofoil Performance, Worcester Polytechnic Institute, December 2007.

[7] Brederode, Vasco de, Fundamentos de Aerodinâmica Incompressível, -1ªed., Lisboa, 1997

[8] Tucker, Vance A., Gliding Birds: Reduction of Induced Drag by Wing Tip Slots Between the Primary Feathers, Department of Zoology, Duke University, Durham, NC 27706, USA, March 1993

[9] Accessed on March 2018, Tekever, URL http://www.tekever.com.

[10] Accessed on October 2019, GE Plastics, Resin Structural Foam Mould, URL http://www.fmcorp.com/downloads/designguide.pdf.